Collective dynamics of kinesin

Adam G. Hendricks* and Bogdan I. Epureanu†
Department of Mechanical Engineering, University of Michigan, Ann Arbor, Michigan, 48109–2125 USA

Edgar Meyhöfer‡
Department of Mechanical Engineering and Department of Biomedical Engineering, University of Michigan, Ann Arbor, Michigan, 48109–2125 USA

(Received 23 September 2008; revised manuscript received 31 January 2009; published 31 March 2009)

Motor proteins are biological enzymes that convert chemical energy to mechanical work in cells. Kinesin-1 is a motor protein that transports vesicles along microtubules and is widely believed to be responsible for anterograde transport of synaptic vesicles in neurons. Advances in single-molecule techniques have shown that single kinesin motors are capable of processive movement along the microtubule at a maximum velocity of approximately 1 μm/s. The velocity decreases roughly linearly in response to load until reaching stall at a load of approximately 6 pN. Several theoretical models have been proposed that describe the steady-state motion of single kinesin motors. Growing evidence suggests that kinesin functions collectively in cells, whereby several motors work in a coordinated manner to transport a vesicle. A transient description is required to describe collective dynamics, as the interactions among coupled motors induce time-varying forces on each motor. Herein a mechanistic model of kinesin is proposed that is capable of accurately describing transient and steady-state dynamics. Each domain of the protein is modeled via a mechanical potential. The mechanical potentials are related explicitly to the chemical kinetics of each motor domain. The mechanistic model was used to simulate the collective behavior of coupled kinesin motors under varying loads, cargo linker stiffnesses, and numbers of motors. To analyze the simulations of coordinated transport, several metrics were developed that are specifically tailored to characterizing the synchronization of nonlinear nonsmooth oscillators such as kinesin. The model results suggest that, in the cell, the dynamics of coupled motors under low loads are loosely correlated. When the load is increased, such as when the cargo encounters an obstacle such as another vesicle or the cytoskeleton, motors become more correlated in response to increased loads, allowing them to produce greater forces. Increasing the number of motors involved in the transport does not appreciably increase the dimension of the trajectory, implying large numbers of motors are able to function in a highly correlated manner without becoming fully synchronized.

DOI: 10.1103/PhysRevE.79.031929 PACS number(s): 87.16.Nn, 82.40.Bj

I. INTRODUCTION

Motor proteins, also called molecular motors or mechanoenzymes, convert chemical energy into structural (conformational) changes, producing mechanical work necessary for a wide range of cellular processes including vesicle transport, cell division, muscle contraction, cell motility, DNA and RNA replications, transcription, and remodeling of macromolecular assemblies [1–4]. One class of motor proteins, kinesins, uses the energy from adenosine triphosphate (ATP) hydrolysis to transport vesicles and organelles along microtubules. It is generally accepted that kinesin-1 uses this movement to transport synaptic vesicles toward the plus end of microtubules in neurons [5]. Single-molecule experiments have characterized the steady-state behavior of kinesin-1, showing a maximum speed of approximately 1 μm/s and a maximum load of 6 pN [6–11]. Despite extensive efforts [12–18], a complete description of the mechanisms kinesin uses to produce movement remains illusive, in particular with respect to cooperativity between motor domains and among groups of motors.

There is considerable evidence that kinesin functions collectively in cells, whereby teams of several kinesin motors, as well as other motor proteins, are involved in the transport of each vesicle [1,3,19]. Recent observations of *in vivo* vesicle trafficking suggest that the cooperation among motors may lead to behavior significantly different from that of single molecules. Researchers have hypothesized the coordination of multiple kinesin motors results in increased step sizes [20], processivity [21], and velocities of up to 10 times the *in vitro* gliding velocity [22,23]. It should be noted that, while intriguing, these observations and their interpretation remain controversial. Diehl *et al.* [24] observed that engineered assemblies of two and three motors increased the speed of gliding assays by a factor of 2 over single motors. In addition to recent experiments, theoretical studies by Badoual *et al.* [25] hypothesized that the directionality in a multiple motor gliding assay is a property of the *ensemble of motor molecules* and not entirely determined by the single-molecule characteristics of a motor molecule. The model of Badoual *et al.* [25], however, is limited to the case where the connections between motors are rigid and the spacing between motors is constrained to be an irrational multiple of the binding site spacing. Several researchers have examined the synchronization of stochastic oscillators [26–31]. For example, Prager *et al.* [32] found that for globally coupled three-state oscillators, the dynamics of the oscillators could

*adhendri@umich.edu
†epureanu@umich.edu
‡meyhofer@umich.edu

become coherent if one of the transitions is deterministic.

An understanding of the mechanism kinesin-1 uses to produce directed movement has numerous potential applications in medicine and nanotechnology. For example, kinesin-1 is implicated in neurological diseases such as Alzheimer's disease and Parkinson's disease [33,34]. An understanding of kinesin-1 may have applications to cancer therapies, as two major drugs used to treat cancer, Taxol and Monastrol, target the function of kinesins [35–37]. Ultimately, the transport machinery of cells could be used to perform targeted drug delivery. Biological motors can also be used to power nanoscale devices, such as for molecular sorting and lab-on-a-chip applications [38–40].

Existing models of motor proteins are not well suited to describing transient dynamics. A transient description is necessary to model coupled motor proteins, as the movement of each motor causes time-varying forces on the coupled motors. Existing models can be classified as kinetic models [14,18,41–44] or thermal ratchet models [13,15–17,45–51]. Kinetic models describe the mechanochemical cycle as a set of discrete states with stochastic, reversible transitions between them. While kinetic models are well suited to describing the steady-state behavior of motor proteins, a quasisteady approximation is made that neglects dynamics at fast time scales. In addition, the dynamics are defined at a small number of discrete spatial locations (2–4 per step in current models). Thus, the force between coupled motors, dependent on the time-varying location of each motor, cannot be resolved. Thermal ratchet models view the motor protein as a single particle or group of particles in stochastically switched potentials. Thermal ratchet models are also well suited for describing the steady-state behavior of motor proteins. However, the potentials must be defined before solving for the motion of the motors. Thus, they cannot account for potentials that are dependent on the instantaneous coupling between motor domains or among multiple motors.

Previously, a deterministic mechanistic model of kinesin-1 was developed and used to study the collective behavior of kinesin motor proteins transporting a common cargo [52]. While the deterministic model gives first-order approximations of the collective dynamics, the dynamics of kinesin-1 are intrinsically stochastic due to the effect of thermal energy on the diffusion of the motor domain between binding sites and the chemical kinetics. Randomness may have a significant effect on the collective behavior. For example, two identical deterministic oscillators with the same initial conditions will follow exactly the same trajectory. However, for stochastic oscillators, the random component of the oscillator dynamics will differ for the two oscillators, such that although the oscillators are identical, their trajectories will differ. Accordingly, while coupled deterministic oscillators can become perfectly phase-locked, stochastic oscillators must overcome random effects to phase lock. It is more likely that stochastic oscillators will, instead of becoming perfectly phase-locked, exhibit fluctuations about a phase-locked state. In this paper, we extend the deterministic model to describe stochastic chemical kinetics, where the time-varying distributions of the chemical dwell time are taken into account. The mechanistic approach presented herein permits an efficient description of the stochastic, collective dynamics of kinesin. Metrics are developed to quantify the synchronization of coupled nonlinear nonsmooth oscillators such as kinesin. With the mechanistic model and metrics of synchronization, we examine the effect of stochasticity on the collective behavior with respect to load, cargo linker stiffness, and the number of motors. The load and the cargo linker stiffness are expected to have an effect on the collective behavior, as these parameters modulate the coupling strength between the motors or the energetic incentive motors gain by synchronizing. Various numbers of motors are examined as intracellular transport is thought to involve teams of two to ten motors [1,19,53].

II. MODEL

The directed movement of kinesin is the combined result of conformational transformations, the relaxation of internal stresses, and Brownian motion. In the proposed model, the mechanochemical cycle proceeds as follows. Beginning with both heads at a binding site, the rear head is weakly bound to the microtubule and the front head is strongly bound to the microtubule. The stresses in the elastic elements and the resulting (unsteady) forces propel the rear head forward. Brownian motion pushes the head the remaining distance to the next binding site, working against the (time and space varying) internal stresses in the molecule. Once the diffusing head reaches the binding site, the head is assumed to have a high affinity to the microtubule. The majority of the time is spent in this mechanochemical state, with both heads having high affinity to the microtubule, but in opposite structural states. After a dwell time corresponding to the chemical kinetics, the structural states of both heads switch and the cycle repeats.

The structure of the kinesin-1 molecule is approximated as shown in Fig. 1. The neck linkers are modeled as elastic elements that connect the motor domains (heads) to the neck. The equilibrium position of these elastic elements is determined by the chemical state of the motor domain. Another elastic element connects the neck to the cargo (bead), approximating the cargo linker. Due to the small length scales of the problem, inertial effects are assumed negligible compared to the viscous forces [2]. With these assumptions, the equations of motion for the bead (subscript b), strongly bound head (subscript s), and neck (subscript n) may be expressed as

$$\gamma_b \dot{x}_b = -F_L + K_b(x_n - x_b), \tag{1}$$

$$\gamma_s \dot{x}_s = K_s(u - x_s) + K_h(\Psi_s - \psi_s), \tag{2}$$

$$\gamma_n \dot{x}_n = -K_b(x_n - x_b) - K_h(\Psi_s - \psi_s) - K_h(\Psi_w - \psi_w), \tag{3}$$

where $\dot{x}$ represents the velocity, x represents the position, u is the position of the binding site, ψ_w and ψ_s designate the current displacement of the weakly bound and strongly bound heads ($\psi_s = x_s - x_n$ and $\psi_w = x_w - x_n$ with the subscript w denoting the weakly bound head), γ is the damping coefficient due to viscosity, F_L is the external load, K_b is the stiffness of the cargo linker, K_h is the stiffness of the neck linker,

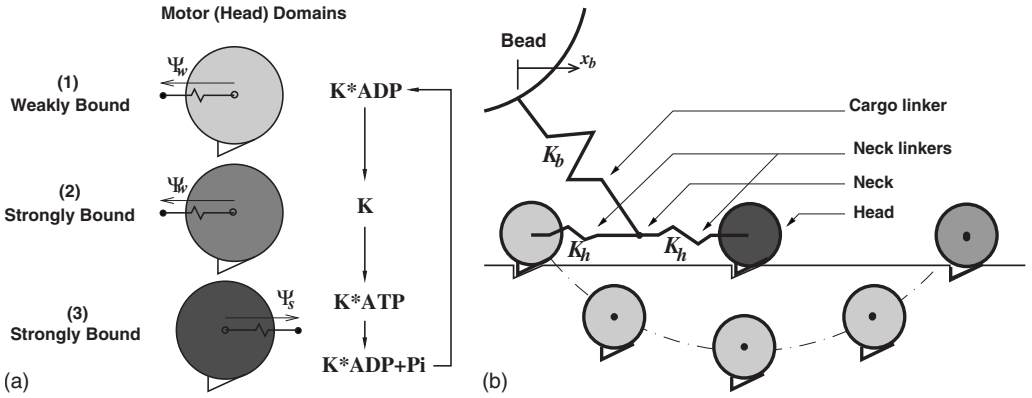

FIG. 1. Each motor domain has three states corresponding to the bound nucleotide. The structural state is described by the equilibrium position of the neck with respect to the head, Ψ, and the affinity to the microtubule binding site. The conformational change (change of structural states) induces stresses in the domains of the molecule, propelling the rearward head forward. Brownian motion then pushes the head to the next unoccupied binding site, where the structural state of the heads switches simultaneously and the cycle is repeated.

and K_s is the stiffness corresponding to the strong affinity to the microtubule in the bound state. The distances Ψ_s and Ψ_w designate the equilibrium position of the neck with respect to the heads (the position when the internal stresses in the molecule are balanced).

The motion of the diffusing head is modeled using an approach based on the mean first-passage time. The mean first-passage time is the average time for a particle to diffuse a prescribed distance in a given potential. The forces on the diffusing weakly bound head (denoted by the subscript w) are due to the internal strain,

$$V_i(\psi_w) = \frac{1}{2}K_h(\Psi_w - \psi_w)^2, \tag{4}$$

and the affinity to the microtubule,

$$V_a(x_w) = \begin{cases} \dfrac{F_w L}{\pi} - \dfrac{F_w L}{\pi}\cos[\pi(u - x_w)/L_a], & \text{if } |x_w - u| < L_a \\ 0, & \text{otherwise,} \end{cases} \tag{5}$$

where F_w is the affinity strength (pN) and L_a is the length (nm) over which the weak binding forces are active. The form chosen for $V_a(x_w)$ approximates a potential well at the binding site corresponding to the affinity of the weakly bound head to the binding site. The value of the parameter F_w which determines the strength of the affinity is based on the kinetic mechanism of Cross [54]. Given these forces, the potential for the diffusing head is

$$V = V_i(\psi_w) + V_a(x_w). \tag{6}$$

However, the forces acting on the diffusing head can vary in time due to unsteady forces on the bead. As the motor motion proceeds, the potential the head has encountered until time t and position x is known. The potential function for the remaining distance to the binding site is estimated based on the motor configuration. Using the known (past) and estimated (future) potentials, an estimated first-passage time is calculated. The mean first-passage time is given by

$$t_0 = \frac{1}{j_0} = \frac{1}{D}\int_0^{x_0} \exp\left[\frac{-V(x)}{k_B T}\right]\left(\int_x^{x_0} \exp\left[\frac{V(y)}{k_B T}\right]dy\right)dx, \tag{7}$$

where D is the diffusion coefficient, x_0 is the distance to the next free binding site (16 nm), k_B is the Boltzmann constant, and T is the absolute temperature [2,55]. Using t_0, one may then calculate the average velocity for the head to reach the binding site at the first-passage time as

$$\dot{x}_w = \frac{x_0 - x}{t_0 - t}. \tag{8}$$

When the time interval between each re-estimation of the varying loads and corresponding potentials decreases, this algorithm converges to the exact mean first-passage time because the estimated potential converges to the exact potential as the head progresses.

The chemical kinetics of the motor protein describe the dwell time corresponding to ATP binding and the conformational change. A model of kinesin dynamics was previously developed by Hendricks *et al.* [52,56] who described the chemical kinetics deterministically. Herein, that work is extended to include stochastic chemical kinetics, whereby the time-varying effect of ATP concentration and internal stresses on the distribution of the chemical dwell time are taken into account. The inclusion of stochasticity is expected to have significant impact on the dynamics of coupled motors. The dwell time associated with the diffusion of the motor domain between binding sites is much shorter than the dwell time due to the chemical kinetics. Hence, only the effect of randomness on the chemical kinetics is considered. The chemical kinetics of each motor domain (head) is assumed to behave according to Michaelis-Menten kinetics, defined by one reversible reaction followed by an irreversible reaction. The rates are defined as

$$k_{1f} = k_{1f,0}, \tag{9}$$

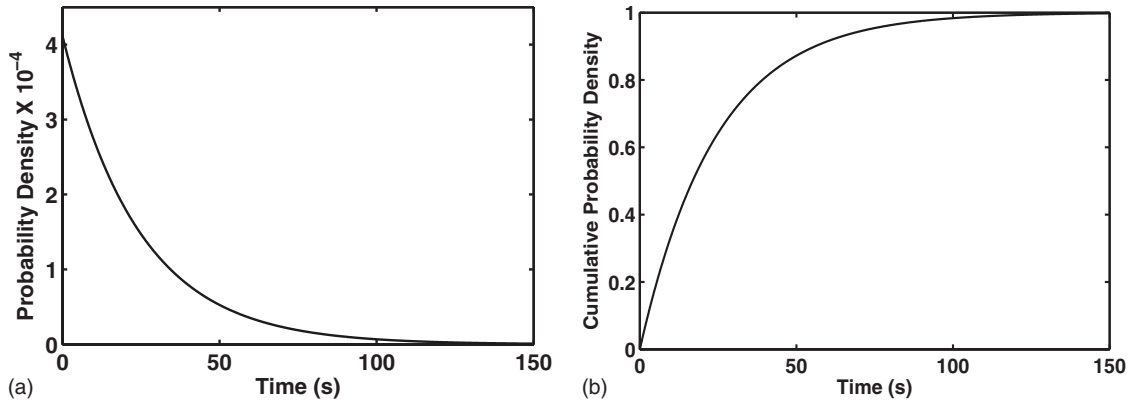

FIG. 2. The probability distributions of the chemical dwell time. For each step of the motor, a uniformly distributed random variable is sampled and used as the value of the cumulative probability for that cycle. While the random variable is constant for each cycle, the distributions are updated at each time step in the simulation.

$$k_{1b} = k_{1b,0} \exp\left[\frac{\frac{1}{2}\kappa|\psi_s - \Psi_c|^{n_c}}{k_B T}\right], \tag{10}$$

$$k_{2f} = k_{2f,0}, \tag{11}$$

where $k_{1f,0}$, $k_{1b,0}$, $k_{2f,0}$, Ψ_c, n_c, and κ are parameters in the model. We assume that there is an optimal molecule configuration for the chemical reaction to proceed, defined by Ψ_c. A configuration away from this optimal configuration presents an energy barrier to the chemical reaction, which is modeled by increasing the effective k_{1b}. From Kou *et al.* [57], the probability density of the chemical dwell time is

$$f(t) = \frac{k_{1f}k_{2f}[\mathrm{ATP}]^*}{2A}[e^{(A+B)t} - e^{(B-A)t}], \tag{12}$$

where

$$A = \sqrt{(k_{1f}[\mathrm{ATP}]^* + k_{1b} + k_{2f})^2/4 - k_{1f}k_{2f}[\mathrm{ATP}]^*} \tag{13}$$

and

$$B = -(k_{1f}[\mathrm{ATP}]^* + k_{1b} + k_{2f})/2. \tag{14}$$

The asterisk denotes that [ATP] is measured in μM (10^{-6} mol/L). The probability distribution is then integrated to get the cumulative probability distribution

$$c(t) = \frac{k_{1f}k_{2f}[\mathrm{ATP}]^*}{2A}\left[\frac{1}{(A+B)}e^{(A+B)t} - \frac{1}{(B-A)}e^{(B-A)t} - \frac{1}{(A+B)} + \frac{1}{(B-A)}\right], \tag{15}$$

which varies from 0 to 1. A uniformly distributed random variable, w, is sampled once for each step of the motor. The probability distribution of the chemical dwell time is computed at each time step in the simulation. The chemical dwell time corresponding to the value of the cumulative probability equal to the random variable for that step is taken as the instantaneous chemical dwell time T_C such that

$$c(T_C) = w_j, \tag{16}$$

where j is the step index. Typical distributions of the chemical dwell time are shown in Fig. 2. Increasing the forward rates (k_{1f} and k_{2f}) shifts the distributions to shorter chemical dwell times, while increasing the backward rate (k_{1b}) shifts the distributions toward longer chemical dwell times.

The heads are assumed to be in opposite structural states at all times, with one head in state (3) and one head in state (1) or (2), as seen in Fig. 1. Therefore, only one variable is required to describe the structural state of both heads. The switching of structural states (corresponding to the chemical or nucleotide states) is assumed to be dependent on the configuration of the motor and also on the ATP concentration. While one head is diffusing, the chemical state variable is approximately constant. Once the diffusing head is within 1% of the distance to the binding site, the rate of change of the chemical state variable is given by

$$\dot{\rho} = \pm \frac{[E]_t}{T_C}, \tag{17}$$

where the total enzyme concentration $[E]_t$ is taken as 5×10^3 μM. To our knowledge, there are no available data for establishing the accuracy of the estimate of 1% of the distance between binding sites (0.08 nm). However, the overall results are only very weakly dependent on this parameter of the model. The chemical state variable, ρ, is considered to grow or decay until it reaches ± 1, at which time the structural states of both heads switch simultaneously.

When multiple motors pull a common cargo, the model assumes that the motors do not sterically interfere with one another or their binding sites. This is equivalent to assuming that the attachment points to the cargo are adequately spaced so that the motors will not interfere with one another while they are mechanically coupled. Therefore, the only coupling between the motors is through the load. Also, the cargo linker is assumed to sustain only forces in tension, not compression. Thus, for N coupled motors the equations for the necks and common cargo are

$$\gamma_n \dot{x}_{n,k} = -F_{b,k} - K_h(\Psi_s - \psi_{s,k}) - K_h(\Psi_w - \psi_{w,k}), \tag{18}$$

TABLE I. Parameter values for the mechanistic model obtained by fitting the model to experimental data in [58].

Parameter	Value	Units
K_h	7.23	pN/nm
F_w	5	pN
K_s	10^4	pN/nm
L_a	0.8	nm
K_b	1	pN/nm
Ψ_s	1.40	nm
Ψ_w	−1.40	nm
Ψ_c	−6.50	nm
n_c	2	
$k_{1f,0}$	53.47	μM s^{-1}
$k_{1b,0}$	2.94×10^3	s^{-1}
$k_{2f,0}$	3.49×10^{-4}	s^{-1}
κ	1.63	pN/nm

$$\gamma_b \dot{x}_b = -F_L + \sum_{k=1}^{N} F_{b,k}, \tag{19}$$

where

$$F_{b,k} = \begin{cases} K_b(x_{n,k} - x_b), & \text{if } x_{n,k} - x_b > 0 \\ 0, & \text{otherwise.} \end{cases} \tag{20}$$

The values of the parameters used in the model were obtained by fitting the model to the single-molecule experimental data of [58]. The parameter values are summarized in Table I. As shown in Fig. 3, the stochastic model fits the steady-state force-velocity data well.

III. METRICS OF SYNCHRONIZATION

A large body of previous work on coupled oscillators has focused on simple one-degree-of-freedom oscillators [59–64]. However, motor proteins are nonsmooth oscillators with multiple time scales in the cycle. The nonsmoothness is caused by the switching in the variables Ψ_s and Ψ_w in Eqs. (1)–(3) and by the tether behavior of the cargo linker in Eq. (20). The multiple time scales are caused by the difference in average velocity during diffusion and during the dwell time. Accordingly, two metrics are proposed that are specifically tailored to quantify the synchronization of coupled nonlinear nonsmooth oscillators.

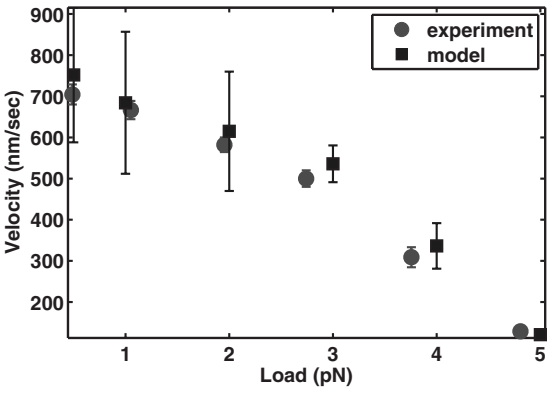

FIG. 3. The stochastic model, using the same values of the parameters as the deterministic model, fits the experimental data from [58] well.

A. Correlation dimension

The dimension of the state space attractor of the dynamics quantifies the degree of synchronization of coupled oscillators. It is expected that when the oscillators are not synchronized, the trajectory in state space is complex and many coordinates are required to describe its evolution. Hence, the dimension of the attractor of the dynamics is high. The maximum of the dimension is the total number of degrees of freedom in the system. Conversely, if the oscillators are perfectly synchronized onto a limit cycle, the dynamics lie on an attractor which can be described by a unique coordinate so that the dimension of the attractor is one. The dimension is a particularly useful measure as it takes into account inherent symmetries in the system, e.g., the period-2 limit cycle behavior of the kinesin motors. Also, the dimension is an invariant of the dynamics and thus remains unchanged irrespective of the coordinates used to describe the system. This is a feature particularly useful for comparing various sets of experimental or computational results in a consistent manner. In its usual definition, the dimension is calculated at steady state. However, we would like to characterize changes in the dimension of the attractor in time. Accordingly, we assume the time scales of changes in the dimension take place slowly relative to the dynamics of the system. The time series can then be broken into intervals of sufficient length to calculate an approximate correlation dimension [65,66]. The trajectory is continuous, so the correlation dimension is calculated based on the length of the trajectory inside a given neighborhood instead of on the usual counting of numbers of points. This results in an efficient and accurate method to calculate the fractal/correlation dimension.

B. Energy analysis

In this section, a method is developed to quantify the amount of energy in the phase-locked mode of coupled oscillators. Here, we use a definition for the modal energy in the dynamics taken from proper orthogonal decomposition analysis. The average modal energy in the dynamics is defined, for a vector $\mathbf{v}$, as

$$E = \frac{1}{T}\int_0^T \frac{1}{2}\mathbf{v}^T(t)\mathbf{v}(t)dt. \tag{21}$$

Modal energy does not directly correlate to a physical energy, but is an energylike quadratic form that includes all states of the dynamic system. If one of the components of v corresponds to a velocity, its contribution to the average modal energy corresponds to the associated average kinetic energy. However, for states such as the chemical state variable, there is no physical corollary to the energy and as such the energy used in this analysis has no relationship to the

amount of energy converted to mechanical work by the motor protein. Nonetheless, this definition of energy is useful when analyzing the dominant dynamics of a system. If the oscillators are phase-locked or the phase difference between the oscillators is constant in time, the fraction of energy in the phase-locked mode to the total amount of energy in the dynamics is close to 1. If the oscillators are not perfectly phase-locked, the fraction is lower. The energy-based method simultaneously solves for the phase difference between oscillators. The calculation proceeds as follows. First, a matrix is constructed of the values of the states of the system at many times

$$X = \begin{bmatrix} \bar{x}_1(t_1) & \bar{x}_1(t_2) & \cdots & \bar{x}_1(t_N) \\ \bar{x}_2(t_1) & \bar{x}_2(t_2) & \cdots & \bar{x}_2(t_N) \\ \vdots & \vdots & \ddots & \vdots \\ \bar{x}_M(t_1) & \bar{x}_M(t_2) & \cdots & \bar{x}_M(t_N) \end{bmatrix}, \tag{22}$$

where $\bar{x}_m(t_n)$ denotes the states of oscillator m at time t_n. Each oscillator is then phase shifted by a time τ_i with respect to oscillator 1 such that

$$X(\bar{\tau}) = \begin{bmatrix} \bar{x}_1(t_1) & \bar{x}_1(t_2) & \cdots & \bar{x}_1(t_N) \\ \bar{x}_2(t_1+\tau_1) & \bar{x}_2(t_2+\tau_1) & \cdots & \bar{x}_2(t_N+\tau_1) \\ \vdots & \vdots & \ddots & \vdots \\ \bar{x}_M(t_1+\tau_{M-1}) & \bar{x}_M(t_2+\tau_{M-1}) & \cdots & \bar{x}_M(t_N+\tau_{M-1}) \end{bmatrix} = [X_1 \quad X_2 \quad \cdots \quad X_N], \tag{23}$$

where $\bar{\tau}=[\tau_1,\tau_2,\cdots,\tau_{M-1}]$ is a vector containing the phase shift of each oscillator with respect to oscillator 1. Next, we seek to transform to a coordinate system that moves with the average velocity of the oscillators. Thus, we define a mode shape of the drift, the component of the dynamics due to the average velocity of the oscillators (i.e., when all states are moving together), as

$$D = [1,1,\ldots,1]^T. \tag{24}$$

We can then subtract the component of dynamics due to the drift and the mean

$$X_n' = X_n - \frac{D^T X_n}{D^T D} D, \tag{25}$$

$$\tilde{X}_n = X_n' - \langle X_n' \rangle. \tag{26}$$

The variables $\tilde{X}_n$ represent fluctuations of zero mean in the moving coordinates which follow the drift motion. For the kinesin model, the states of each motor (oscillator) are defined as

$$\bar{x}_m = [x_{\text{head1}},\ x_{\text{head2}},\ x_{\text{neck}},\ \rho]^T, \tag{27}$$

where the states are defined by the position of head 1, the position of head 2, the position of the neck, and the chemical state variable. On the moving coordinate frame that follows the average motion of the molecule, synchronous motion will occur when head 1 of each motor is moving forward, head 2 is moving backward, the hinge is stationary, and the chemical state variable is constant. Thus, we define the mode shape of the synchronous motion for each motor as

$$\bar{s}_m = [1,\ -1,\ 0,\ 0]^T. \tag{28}$$

The mode shape of synchronous motion for the collection of oscillators is then

$$S = [\bar{s}_1^T,\ \bar{s}_2^T,\ \cdots,\ \bar{s}_M^T]^T. \tag{29}$$

From the definition in Eq. (21) for small time intervals $(t_n - t_{n-1})$, the total energy in the dynamics can be approximated as

$$E_{\text{tot}} = \frac{1}{2T_{\text{tot}}} \sum_{n=1}^{N} \Delta t (\tilde{X}_n^T \tilde{X}_n), \tag{30}$$

where $\Delta t = t_n - t_{n-1}$ and $T_{\text{tot}} = \Sigma_{n=1}^{N} \Delta t$. We now seek the component of the energy along the vector S or the energy in the phase-shifted mode. The projection of $\tilde{X}_n$ along S is given by

$$\tilde{X}_n^{\parallel} = \frac{S^T X_n}{S^T S} S. \tag{31}$$

The energy in the phase-shifted mode is then

$$E_{\text{ps}}(\bar{\tau}) = \frac{1}{2T_{\text{tot}}} \sum_{n=1}^{N} \Delta t [(\tilde{X}_n^{\parallel})^T (\tilde{X}_n^{\parallel})] = \frac{1}{2T_{\text{tot}}} \sum_{n=1}^{N} \Delta t \frac{(S^T \tilde{X}_n)^2}{S^T S}. \tag{32}$$

Finally, an optimization routine is used to find the time delays, $\bar{\tau}$, that correspond to the maximum energy in the phase-shifted mode. The optimization routine minimizes the cost function

$$C(\bar{\tau}) = 1 - \frac{E_{\text{ps}}}{E_{\text{tot}}}. \tag{33}$$

The cost function is shown as a function of the phase $\bar{\tau}$ for two coupled motor proteins in Fig. 4 where $\bar{\tau}$ has only one entry, i.e., it is a scalar. If the cost function is minimum at $\bar{\tau}$, the function will also be minimum at $\bar{\tau}+T$, where T is the period of the oscillator. Thus, we choose the phase where the magnitudes of both $\bar{\tau}$ and the cost function are minimum.

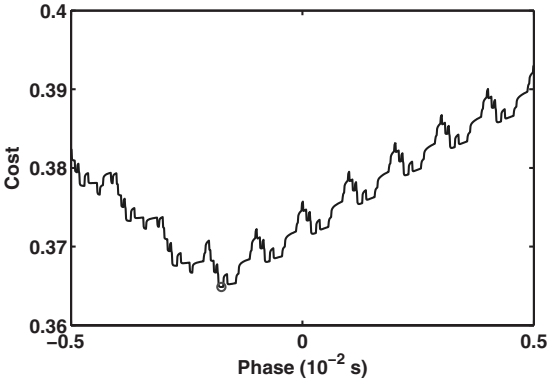

FIG. 4. The cost function [Eq. (33)] as a function of phase calculated for the simulated dynamics of two coupled motors. An optimization routine is used to find the minimum of the cost function, which corresponds to the maximum energy in the phase-locked mode.

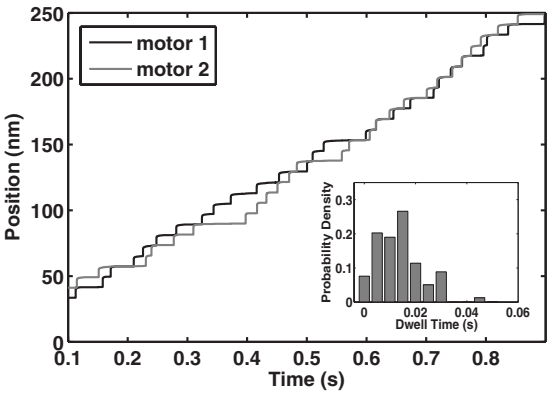

FIG. 5. Typical simulated movement of two coupled motors transporting a common cargo. The neck locations (the centroids) of the motors are shown. The stochastic model exhibits a distribution of dwell times.

The energy analysis results in the fraction of energy in the phase-locked mode and the phase between oscillators.

IV. RESULTS

The mechanistic model presented in this paper describes the transient stochastic dynamics of kinesin, making it well suited to study the collective behavior of multiple motors transporting a common cargo. A typical prediction of the stochastic model for two coupled motors is shown in Fig. 5. The stochastic chemical kinetics affect the collective dynamics as the motors are perturbed away from a phase-locked state by stochastic fluctuations. To become fully synchronized, the coupling forces would have to overcome the fluctuations from the chemical kinetics. In this section, the metrics presented in Sec. III are used to investigate the collective dynamics of coupled kinesin motors, with respect to the cargo linker stiffness, load, and the number of motors. For each case, the data consist of ten independent simulations of 50 steps each.

A. Effect of cargo linker stiffness

The stiffness of the cargo linker directly affects the coupling strength or the energetic advantage the motors gain by synchronizing. As the stiffness increases, a difference in the strain of the cargo linkers of coupled motors translates to a larger difference in the load each motor carries. For example, if the cargo linker stiffness is 0.1 pN/nm and the difference in strain of the cargo linkers is 1 nm, the difference in load of the two motors is 0.1 pN. If the stiffness is increased to 1 pN/nm, the difference in the load is increased to 1 pN. Thus, it is expected that the motors will tend to synchronize as the cargo linker stiffness is increased. The results of the model are consistent with this expectation, as is shown in Fig. 6. The fraction of energy in the phase-locked mode increases as the stiffness increases. The effect is more pronounced at higher loads, as higher loads increase the incentive to synchronize. The correlation dimension also increases with cargo linker stiffness, indicating that while the motors become more synchronized (i.e., spatially coherent), the trajec-

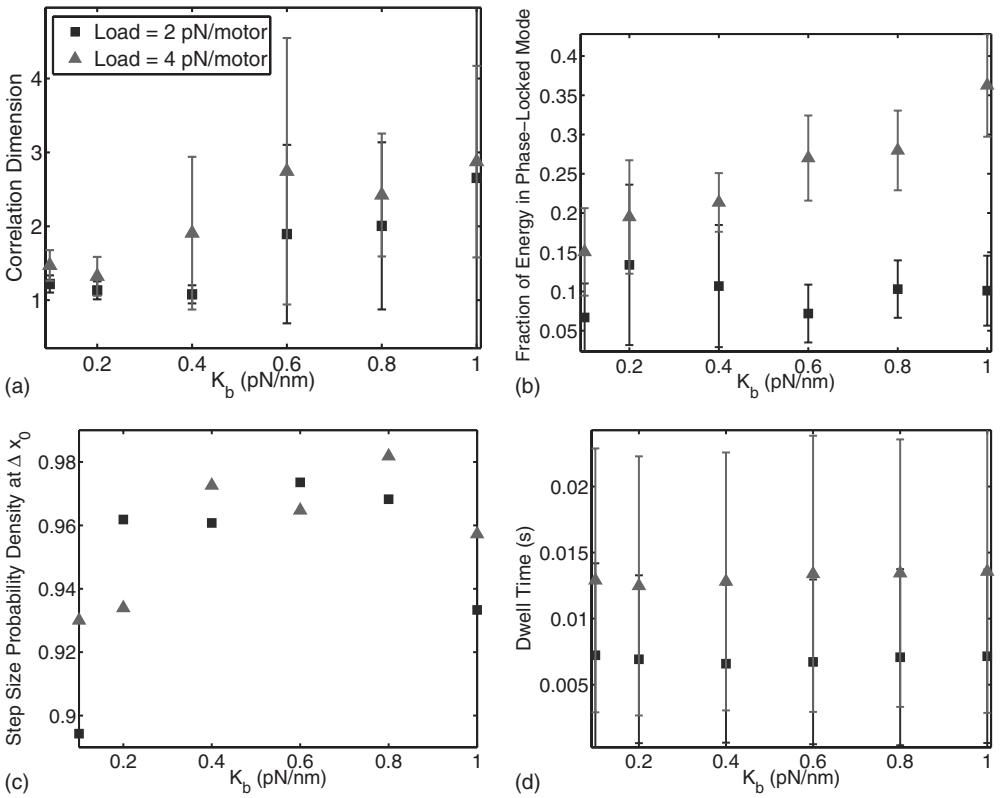

FIG. 6. The effect of cargo linker stiffness, K_b, on the collective dynamics of two kinesin motors transporting a common cargo. Bars indicate the standard deviation. Legend: (■) Load=2 pN/motor, (▲) Load=4 pN/motor.

tory becomes more complicated temporally. The standard deviation of the correlation dimension, shown by the error bars, also increases with the cargo linker stiffness, indicating that stochasticity affects the trajectories more at higher cargo linker stiffness. In summary, the dynamics of the motors become more correlated with increasing load, while the trajectory of the motors becomes more complex in time. Step size distributions were calculated using the cumulated step size data from all runs and using a bin size of 0.5 nm. The value of the probability density of the step size distributions at the expected step size Δx_0 is shown in Fig. 6. The expected step size is taken as $\Delta x_0 = (8\ \text{nm})/(\text{number of motors})$. For example, the step size of the cargo when transported by a single kinesin motor is 8 nm. If two motors are transporting a cargo and they are not stepping in synchrony, then the cargo will advance 4 nm each time one of the motors steps. The value of the probability density of the step size distributions at Δx_0 increases as the motors become more synchronized, indicating that the distribution narrows. At the highest stiffness, the probability density at Δx_0 decreases as the distribution broadens. This suggests that complexity in the trajectory, indicated by increases in the correlation dimension, causes the step size distribution to broaden while correlation between the motors, indicated by increases in the fraction of the energy in the phase-locked mode, causes the step size distribution to narrow.

B. Effect of load

Like the effect of the cargo linker stiffness, the load also increases the coupling strength. The slope of the force-velocity curve increases from approximately 50 nm/s/pN for loads below 2 pN to approximately 200 nm/s/pN at loads greater than 3 pN. Therefore, for a given difference in the loads between motors, the difference in the average velocity of the two motors will increase with the load on the cargo. As shown in Fig. 7, the load increases the coupling strength, which in turn increases the amount of energy in the phase-locked mode. Analogous to the effect of increasing the coupling strength through the cargo linker stiffness, the correlation dimension also increases with load, indicating trajectories are more complex temporally at high loads. Load also increases the effect of stochasticity on the dynamics, as the standard deviation of the fraction of energy in the phase-locked mode and the correlation dimension increases with load. The results suggest that even for many coupled motors, the velocity is strongly correlated with the load per motor. The step size distribution narrows as the load is increased, evidenced by the value of the probability density at Δx_0 increasing with load.

C. Effect of number of motors

While the coupling strength is proportional to the cargo linker stiffness and the load, the number of motors does not affect the coupling strength. However, the chemical kinetics of each motor is dependent on random processes that are independent for each motor. Thus, each motor represents the addition of an independent random process to the system, suggesting that the degree of synchronization should decrease with the number of motors. As shown in Fig. 8, the fraction of energy in the phase-locked mode decreases with the number of motors. Alternatively, one may argue that because the velocity of the cargo becomes more constant as the number of motors increases, the forces on the motors must also become more constant, implying greater synchronization. However, while it is true that the total force on the cargo (i.e., the sum of the forces on all of the motors) becomes more constant with greater numbers of motors, the variance of the forces on each individual motor need not decrease. Consider the force $F=f_1+f_2$. There are many cases where f_1 and f_2 can vary in time, but sum such that F is constant. Although the fraction of energy in the phase-locked mode decreases with the number of motors, the correlation dimension is not appreciably affected by the number of motors (the variation is within the standard deviation), indicating that the trajectory remains similar as the number of motors is increased. The value of the correlation dimension of approximately 1.5 indicates that the trajectory, in a specific coordinate system, lies on a torus. Taken together, the correlation dimension and energy analysis indicate that the dynamics of coupled motors are correlated. However, the energy analysis, which only considers constant phase differences between the motors, indicates a small fraction of the energy is in the phase-locked mode. This suggests that the correlation between the motors cannot be described by a constant phase between each motor, but is likely due to a time-varying periodic phase between the motors. The step size distribution narrows with the number of motors, indicating that the step size distribution narrows as the correlation dimension decreases, as in Fig. 6. The mean step size decreases with the number of motors, indicating the motors are not fully synchronized (phase-locked with a phase difference of 0), in agreement with the correlation dimension and energy analyses.

V. DISCUSSION

The goal of this work was to develop a stochastic model capable of predicting the dynamics of kinesin motors coupled to a shared load. Toward this goal, a deterministic model developed previously by the authors [52,56] was extended to include stochastic chemical kinetics, yielding a stochastic model capable of describing the transient dynamics of kinesin. The resulting model is therefore well suited to investigate the collective behavior of kinesin. While coupled deterministic motors are able to phase lock at certain conditions [56], stochastic motors tend to fluctuate about a phase-locked state as a result of competing forces. The coupling force drives the motors to a phase-locked state, while fluctuations due to the stochastic chemical kinetics perturb the motors away from the phase-locked state. The predictions made by the mechanistic model suggest that the degree of synchronization of coupled kinesin motors is dependent on the mechanical properties of the motors, the load, and the number of motors involved in the transport. While the motors never completely synchronize, the degree of synchronization increases when the coupling strength is increased either through the cargo linker stiffness or the load. At low

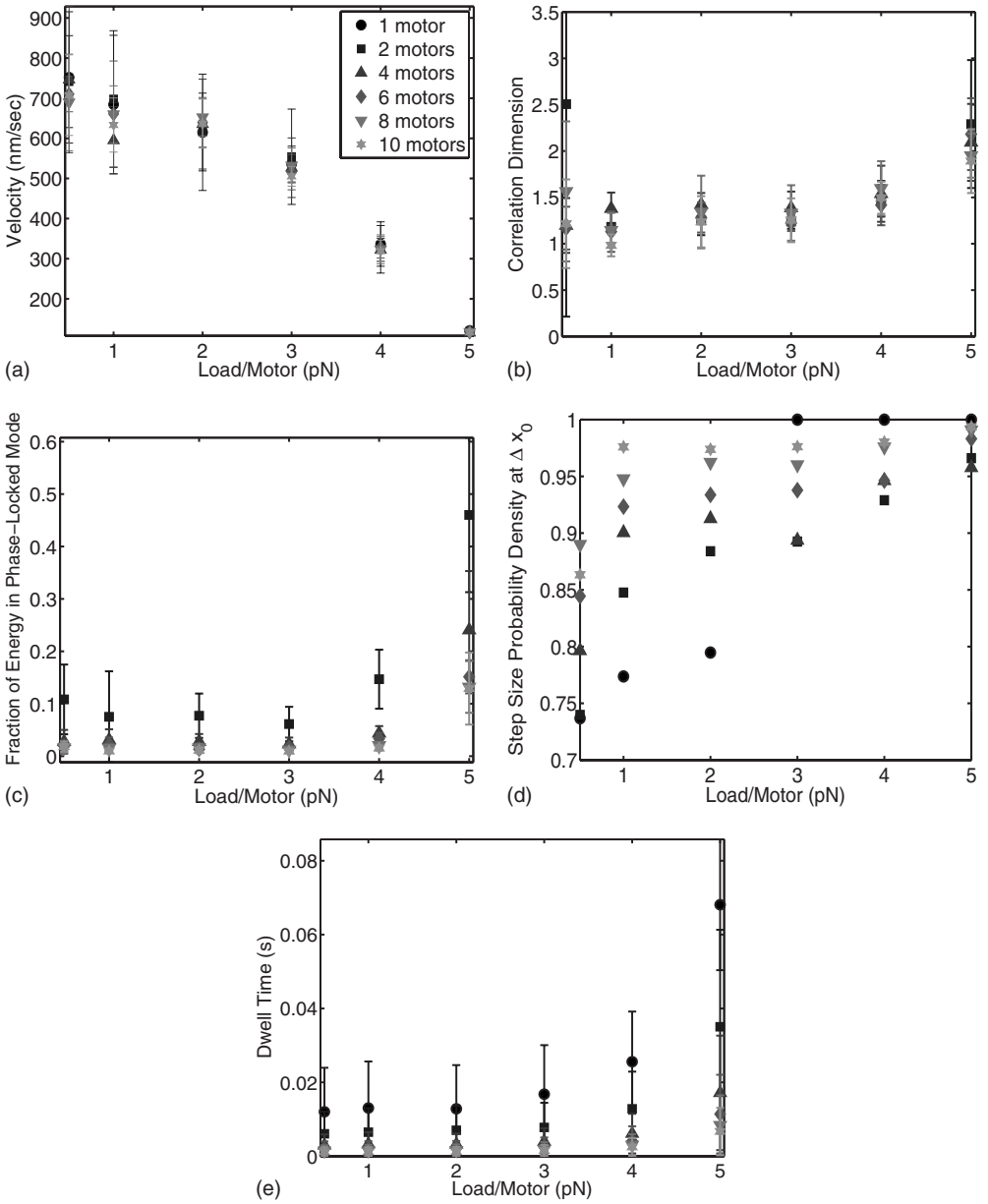

FIG. 7. The effect of the load on the collective dynamics of several kinesin motors, with cargo linker stiffness K_b=0.1 pN/nm, transporting a common cargo. Bars indicate the standard deviation. Legend: (●) 1 motor, (■) 2 motors, (▲) 4 motors, (♦) 6 motors, (▼) 8 motors, and (*) 10 motors.

loads, the motors are loosely coupled and do not synchronize. However, higher loads increase the coupling strength and cause the degree of synchronization to increase, augmenting the efficiency and the maximum force exerted. This result likely holds corollaries for transport in the cell, where motor proteins are expected to be under low load when transporting cargos and their dynamics are loosely correlated. When the cargo encounters an obstacle such as the cytoskeleton or collisions with other vesicles, the dynamics of the motors become better correlated in response to higher loads, allowing them to overcome the obstacle.

The behavior of coupled motors in response to load also points to an advantage that kinesin gains by functioning collectively. Kinesin motors are coupled in such a way that they do not interfere with each other during normal transport. However, when they encounter an obstacle, they can become more synchronized to produce greater forces. Unfortunately, current experimental observations of intracellular transport do not provide a measurement of the load. Likewise, the cargo linker stiffness of kinesin has not been measured accurately. Data from future experiments are therefore needed to refine the predictions of the model.

Current experiments estimate intracellular transport is driven by teams of two to ten motors [1,19,53]. The results of the model indicate that the degree of synchronization decreases with the number of motors, as evidenced by the decrease in the fraction of energy in the phase-locked mode with increasing numbers of motors. At the same time, the dimension of the trajectory does not appreciably increase with the number of motors, suggesting that several motors

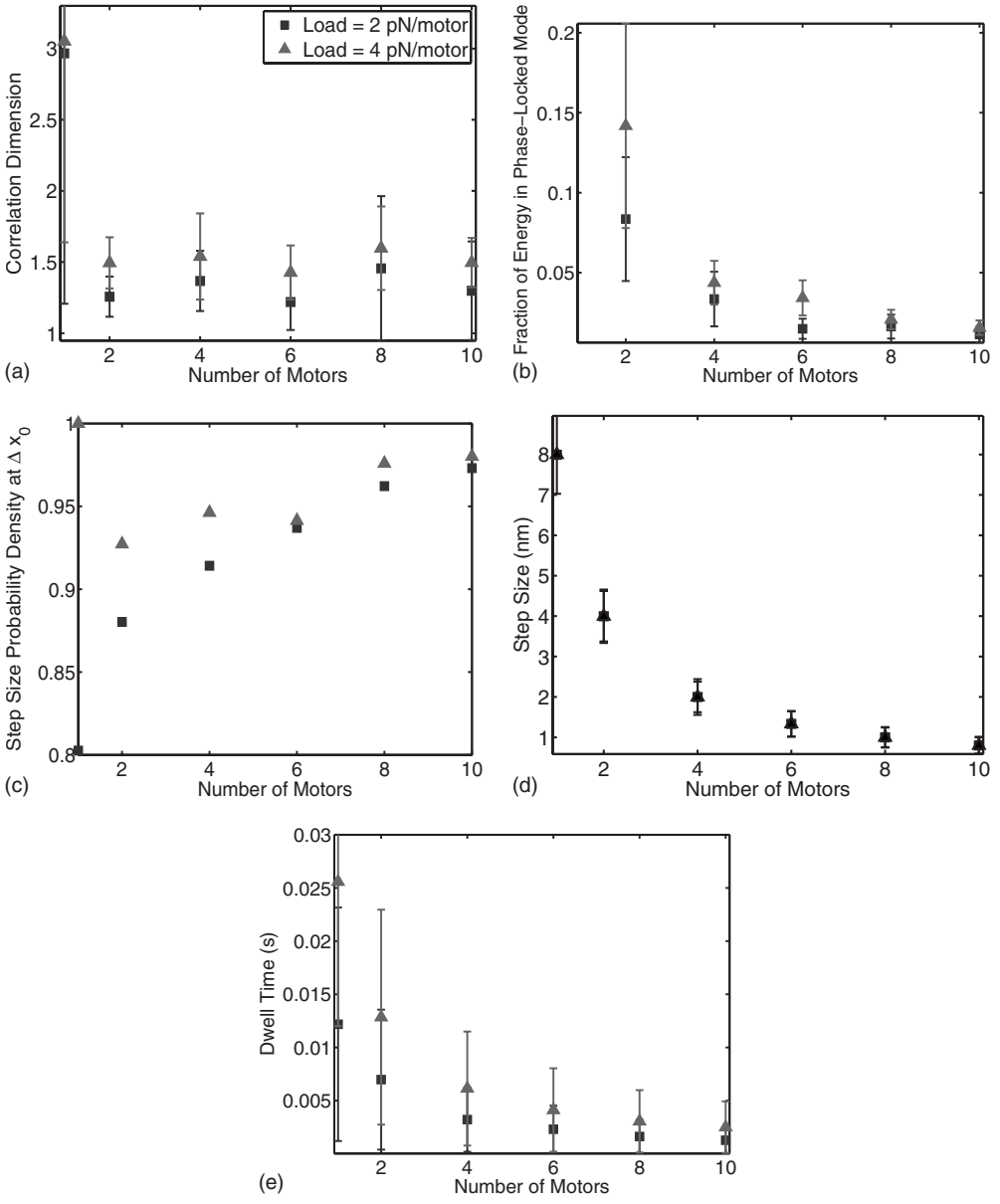

FIG. 8. The effect of the number of motors (K_b=0.1 pN/nm) on the collective dynamics of kinesin. Bars indicate the standard deviation. Legend: (■) Load=2 pN/motor, (▲) Load=4 pN/motor.

interact such that their motion is highly correlated, but cannot be described by a constant phase lag between motors. The correlation dimension suggests that although several coupled kinesin motors do not fully synchronize, their dynamics are highly correlated, allowing several motors to function collectively such that the speed of the transport is not degraded. This points to a periodic, time-varying phase between the motors.

Several researchers made *in vivo* observations of transport directed toward the plus end of the microtubule at velocities faster than the maximum velocities of kinesin observed for single molecules *in vitro* [20–23]. Velocities of up to ten times the single-molecule velocity have been reported in some *in vivo* experiments tracking vesicle movement [22], suggesting that greater velocities may be due to the coordination of many kinesin motors. Our modeling work is not consistent with such observations. The results of the mechanistic model predict that the force-velocity curve for coupled motors is very similar to the single-molecule force-velocity curve when the velocity is plotted against the average load per motor, as shown in Fig. 7. Several explanations may account for this discrepancy. For example, there may have been motors other than kinesin-1 involved in the transport of vesicles *in vivo* or as yet unidentified proteins that upregulate the activity of kinesin-1. Also, in some studies, the observed increases in velocities were observed infrequently and over short distances (20 nm) as expected from short-term diffusive events [22]. Alternately, the fundamental head-to-head coupling of kinesin may change when in a multiple-motor orientation, resulting in a dramatic increase in velocity, or that larger numbers of motors than studied here (greater than 10) are involved in the transport *in vivo*.

The model results put forth several quantitative predictions of the collective dynamics of kinesin that can now be

tested experimentally. First, the model predicts that the force-velocity curve for multiple coupled motors transporting a load closely matches the single-molecule force-velocity curve when the velocity is plotted against the average load per motor. In addition, the relationship between the correlation dimension and cargo linker stiffness, load, and number of motors can be compared to force-clamp measurements of transport by multiple kinesin motors. Note that the correlation dimension can be calculated from the record of the bead locations in time using embedded coordinates [65]. Step size distributions and dwell time distributions can also be compared to experiment using a step-finding algorithm such as the one used by Kerssemakers *et al.* [67]. To test these predictions, careful observations of transport by multiple motors are needed. For comparison to theoretical models, it is essential to measure the number of motors involved in the transport as well as the mechanical properties (e.g., cargo linker stiffness). Observations of a known number of motors transporting a cargo at a known load would severely constrain theoretical models of collective transport. In addition, it may be possible to modulate the coupling between motors by engineering constructs with different cargo linker stiffnesses by, for example, inserting different lengths of a coiled-coil domain into the cargo linker.

The model proposed herein assumes that the mechanisms of kinesin do not change fundamentally when functioning collectively, i.e., the mechanisms of each motor involved in coordinated transport are synonymous with the single-molecule operation, with the exception of time-varying loads induced on each motor through their interaction. Comparisons of the results of the model to experiment have the potential to elucidate a fundamental question of intracellular transport: Are the single-molecule mechanisms of kinesin, such as head-to-head coordination, analogous to the collective mechanisms of kinesin motors, or do coupled motors exhibit a distinct mode of movement responsible for the increased velocities observed *in vivo*?

ACKNOWLEDGMENTS

This material is based upon work supported by the National Science Foundation.

[1] S. Gunawardena and L. S. B. Goldstein, J. Neurobiol. **58**, 258 (2004).
[2] J. Howard, *Mechanics of Motor Proteins and the Cytoskeleton* (Sinauer Associates, Sunderland, Massachusetts, 2001).
[3] R. D. Vale, J. Cell Biol. **163**, 445 (2003).
[4] R. D. Vale, T. S. Reese, and M. P. Sheetz, Cell **42**, 39 (1985).
[5] S. T. Brady, Nature (London) **317**, 73 (1985).
[6] C. L. Asbury, A. N. Fehr, and S. M. Block, Science **302**, 2130 (2003).
[7] C. M. Coppin, D. W. Peirce, L. Hsu, and R. D. Vale, Proc. Natl. Acad. Sci. U.S.A. **94**, 8539 (1997).
[8] E. Meyhöfer and J. Howard, Proc. Natl. Acad. Sci. U.S.A. **92**, 574 (1995).
[9] K. Svoboda and S. M. Block, Cell **77**, 773 (1994).
[10] K. Visscher, M. J. Schnitzer, and S. M. Block, Nature (London) **400**, 184 (1999).
[11] A. Yildiz, M. Tomishige, R. D. Vale, and P. R. Selvin, Science **303**, 676 (2004).
[12] M. J. Schnitzer, K. Visscher, and S. M. Block, Nat. Cell Biol. **2**, 718 (2000).
[13] M. Bier, Contemp. Phys. **46**, 41 (2005).
[14] M. E. Fisher and A. B. Kolomeisky, Proc. Natl. Acad. Sci. U.S.A. **98**, 7748 (2001).
[15] R. F. Fox and M. H. Choi, Phys. Rev. E **63**, 051901 (2001).
[16] R. Kanada and K. Sasaki, Phys. Rev. E **67**, 061917 (2003).
[17] S. Klumpp, A. Mielke, and C. Wald, Phys. Rev. E **63**, 031914 (2001).
[18] C. S. Peskin and G. Oster, Biophys. J. **68**, 202 (1995).
[19] S. P. Gross, M. C. Tuma, S. W. Deacon, A. S. Serpinskaya, A. R. Reilein, and V. I. Gelfand, J. Cell Biol. **156**, 855 (2002).
[20] X. Nan, P. A. Sims, P. Chen, and X. S. Xie, J. Phys. Chem. B **109**, 24220 (2005).
[21] S. Courty, C. Luccardini, Y. Bellaiche, G. Cappello, and M. Dahan, Nano Lett. **6**, 1491 (2006).
[22] C. Kural, H. Kim, S. Syed, G. Goshima, V. I. Gelfand, and P. R. Selvin, Science **308**, 1469 (2005).
[23] V. Levi, A. S. Serpinskaya, E. Gratton, and V. I. Gelfand, Biophys. J. **90**, 318 (2006).
[24] M. R. Diehl, K. Zhang, H. J. Lee, and D. A. Tirrell, Science **311**, 1468 (2006).
[25] M. Badoual, F. Julicher, and J. Prost, Proc. Natl. Acad. Sci. U.S.A. **99**, 6696 (2002).
[26] L. Gammaitoni, P. Hänggi, P. Jung, and F. Marchesoni, Rev. Mod. Phys. **70**, 223 (1998).
[27] D. J. Gauthier and J. C. Bienfang, Phys. Rev. Lett. **77**, 1751 (1996).
[28] T. Risler, J. Prost, and F. Julicher, Phys. Rev. E **72**, 016130 (2005).
[29] J. N. Teramae and Y. Kuramoto, Phys. Rev. E **63**, 036210 (2001).
[30] E. I. Volkov, E. Ullner, and J. Kurths, Chaos **15**, 023105 (2005).
[31] K. Wiesenfeld and F. Moss, Nature (London) **373**, 33 (1995).
[32] T. Prager, B. Naundorf, and L. Schimansky-Geier, Physica A **325**, 176 (2003).
[33] L. S. B. Goldstein, Proc. Natl. Acad. Sci. U.S.A. **98**, 6999 (2001).
[34] G. B. Stokin *et al.*, Science **307**, 1282 (2005).
[35] P. B. Schiff, J. Fant, and S. B. Horwitz, Nature (London) **277**, 665 (1979).
[36] T. U. Mayer, T. M. Kapoor, S. J. Haggarty, R. W. King, S. L. Schreiber, and T. J. Mitchison, Science **286**, 971 (1999).
[37] T. M. Kapoor, T. U. Mayer, M. L. Coughlin, and T. J. Mitchison, J. Cell Biol. **150**, 975 (2000).
[38] H. Hess, Science **312**, 860 (2006).
[39] C.-T. Lin, M.-T. Kao, K. Kurabayashi, and E. Meyhöfer, Small **2**, 281 (2006).
[40] M. G. L. van den Heuvel, M. P. de Graaff, and C. Dekker,

Science **312**, 910 (2006).
[41] M. E. Fisher and A. B. Kolomeisky, Physica A **274**, 241 (1999).
[42] D. Keller and C. Bustamante, Biophys. J. **78**, 541 (2000).
[43] M. E. Fisher and Y. C. Kim, Proc. Natl. Acad. Sci. U.S.A. **102**, 16209 (2005).
[44] A. B. Kolomeisky, E. B. Stukalin, and A. A. Popov, Phys. Rev. E **71**, 031902 (2005).
[45] R. D. Astumian, Science **276**, 917 (1997).
[46] R. D. Astumian and I. Derenyi, Biophys. J. **77**, 993 (1999).
[47] M. Bier, Contemp. Phys. **38**, 371 (1997).
[48] F. Julicher and J. Prost, Phys. Rev. Lett. **78**, 4510 (1997).
[49] K. B. Zeldovich, J. F. Joanny, and J. Prost, Eur. Phys. J. E **17**, 155 (2005).
[50] M. Bier, *Third International Conference on Unsolved Problems of Noise and Fluctuations in Physics, Biology, and High Technology*, AIP Conf. Proc. No. 655 (AIP, New York, 2003), pp. 290–297.
[51] F. Jülicher, Physica A **369**, 185 (2006).
[52] A. G. Hendricks, B. I. Epureanu, and E. Meyhöfer, Nonlinear Dyn. **53**, 303 (2008).
[53] R. D. Vale, Cell **112**, 467 (2003).
[54] R. A. Cross, Trends Biochem. Sci. **29**, 301 (2004).
[55] H. C. Berg, *Random Walks in Biology* (Princeton University Press, Princeton, NJ, 1993).
[56] A. G. Hendricks, B. I. Epureanu, and E. Meyhöfer, Physica D **238**, 677 (2009).
[57] S. C. Kou, B. J. Cherayil, W. Min, B. P. English, and X. S. Xie, J. Phys. Chem. B **109**, 19068 (2005).
[58] S. M. Block, C. L. Asbury, J. W. Shaevitz, and M. J. Lang, Proc. Natl. Acad. Sci. U.S.A. **100**, 2351 (2003).
[59] A. Jadbabaie, N. Motee, and M. Barahona, *Proceedings of the 42nd IEEE American Control Conference* (IEEE, Boston, Massachusetts, 2004), pp. 4296–4301.
[60] Y. Kuramoto, *Chemical Oscillations, Waves, and Turbulence* (Springer, New York, 1984).
[61] R. E. Mirollo and S. H. Strogatz, Physica D **205**, 249 (2005).
[62] A. Pikovsky, M. Rosenblum, and J. Kurths, *Synchronization: A Universal Concept in Nonlinear Science*, Cambridge Nonlinear Sciences Series 12 (Cambridge University Press, London, 2001).
[63] S. H. Strogatz, Physica D **143**, 1 (2000).
[64] S. H. Strogatz and I. Stewart, Sci. Am. **269**, 68 (1993).
[65] S. H. Strogatz, *Nonlinear Dynamics and Chaos* (Perseus, Cambridge, Massachusetts, 1994).
[66] P. Grassberger and I. Procaccia, Physica D **9**, 189 (1983).
[67] J. W. Kerssemakers, E. L. Munteanu, L. Laan, T. L. Noetzel, M. E. Janson, and M. Dogterom, Nature (London) **442**, 709 (2006).